



**HAL**  
open science

## Combustion Kinetics of Alternative Jet Fuels, Part-I: Experimental Flow Reactor Study

Patrick Osswald, Julia Zinsmeister, Trupti Kathrotia, Máira Alves-Fortunato,  
Victor Burger, Rina van Der Westhuizen, Carl Viljoen, Kalle Lehto, Reetu  
Sallinen, Kati Sandberg, et al.

► **To cite this version:**

Patrick Osswald, Julia Zinsmeister, Trupti Kathrotia, Máira Alves-Fortunato, Victor Burger, et al..  
Combustion Kinetics of Alternative Jet Fuels, Part-I: Experimental Flow Reactor Study. *Fuel*, 2021,  
302, pp.120735. 10.1016/j.fuel.2021.120735 . hal-03436502

**HAL Id: hal-03436502**

**<https://ifp.hal.science/hal-03436502>**

Submitted on 19 Nov 2021

**HAL** is a multi-disciplinary open access archive for the deposit and dissemination of scientific research documents, whether they are published or not. The documents may come from teaching and research institutions in France or abroad, or from public or private research centers.

L'archive ouverte pluridisciplinaire **HAL**, est destinée au dépôt et à la diffusion de documents scientifiques de niveau recherche, publiés ou non, émanant des établissements d'enseignement et de recherche français ou étrangers, des laboratoires publics ou privés.



30 consists of an atmospheric flow reactor with coupled molecular-beam mass spectrometer (MBMS).  
31 Quantitative evolution of combustion reaction intermediates is recorded for fuel-rich ( $\Phi=1.2$ ) and  
32 fuel-lean ( $\Phi=0.8$ ) conditions at intermediate temperatures up to 1200K including small intermediate  
33 species (e.g. ethylene, butene) and soot precursor species (e.g. benzene, naphthalene, phenanthrene).  
34 A general systematic dependency of the soot precursor concentration on the degree of unsaturation  
35 (Index of Hydrogen Deficiency) or the hydrogen content, respectively, is demonstrated. Furthermore,  
36 larger soot precursor concentrations depend on the naphthalene content of the fuel.

### 37 **Keywords**

38 Technical Jet Fuels, Synthetic Fuels, Speciation, Soot Precursor, Laminar Flow Reactor, Combustion  
39 Kinetics

40

## Highlights “Combustion Kinetics of Alternative Jet Fuels, Part-I: Experimental Flow Reactor Study”

- Systematic insights into combustion chemistry of 42 chemically complex jet fuels.
- Experimental speciation data (by MBMS) for kinetic model development.
- Fuel’s chemical composition significantly affects the soot precursor species pool.
- Soot precursor chemistry depends on fuel’s degree of unsaturation/hydrogen content.
- Larger aromatic soot precursors depend on fuel’s naphthene content.

## 1. Introduction

High requirements regarding safety together with weight limitation and long lifetime of aircrafts make aviation one of the most difficult sectors to decarbonize. The industry relies on synthesized carbon neutral fuels (SAF: Sustainable Alternative Fuel) to achieve their climate goals. Even though alternative technologies such as electric- or hydrogen-powered aircrafts are envisaged as long-term perspectives, there is no other option available for long-distance flights in the mid-term. Consequently, several pathways for producing carbon-neutral aviation fuels from renewable feedstocks are currently investigated [1-3].

The specification for synthetic turbine fuels (ASTM-D7566) allows blending up to 50vol% of synthetic components to conventional crude oil-based fuel (ASTM-D1655). In particular specification of new synthetic routes is a highly dynamic field. By the end of 2020 seven synthetic blend-stocks have been annexed to the ASTM-D7566-20b: a) Synthesized Paraffinic Kerosene (SPK), produced by Fischer-Tropsch (FT) synthesis from various feedstocks, b) Hydroprocessed Esters and Fatty Acids (HEFA) gained from mono-, di-, and triglycerides, free fatty acids or fatty acid methyl esters, c) Synthesized Iso-Paraffins (SIP) produced from hydroprocessed fermented sugars via biotechnological processes. SIP is currently limited to 10vol% blending fraction. d) Synthesized Paraffinic Kerosene plus Aromatics (SPK/A) are FT-Paraffins with addition of nonpetroleum alkylated light aromatics. e) Alcohol-To-Jet Synthetic Paraffinic Kerosene (ATJ-SPK) produced by dehydration, oligomerization and hydrogenation from biotechnologically accessible alcohols (currently isobutanol and ethanol), f) Catalytic Hydrothermolysis Jet (CHJ) fuel based on a hydrothermal conversion and hydrotreating operations of fats, oils and grease feedstocks, and g) Hydroprocessed Hydrocarbons, Esters and Fatty Acids (HC-HEFAs) that incorporate biomass from specific sourced, to date from algae (*Botryococcus braunii*). HC-HEFA is also limited to 10vol%. In addition, Sasol's Semi- and Fully-Synthetic Jet Fuel (SSJF and FSJF) from the Secunda plant in South Africa is annexed to the UK MoD DEF-STAN 91-091 specification as well as to ASTM-D1655.

67 While carbon dioxide emission savings primarily depend on the feedstock of the SAF production,  
68 many have shown their ability to reduce the particulate emission of various aero engines in ground  
69 and flight tests e.g. [4-6]. This is of particular interest when non-CO<sub>2</sub> climate effects like contrail  
70 formation [7] or local airport air quality are considered [8]. The effect is typically assigned to the  
71 reduction of the aromatic content [9] of the fuel when blended with aromatic free synthetic  
72 components. More recent experiments indicate the fuel's hydrogen content being a better parameter  
73 to predict the soot emission of a fuel than the aromatic content [5, 10, 11].

74 With the implementation of alternative fuels, the need of chemical kinetic models for correct  
75 prediction of the aforementioned fuel effects is increasing [12]. A successful approach is presented  
76 with the HyChem model developed at Stanford University [13, 14]. However, when combustion  
77 kinetics is considered, the complexity of technical fuels, that typically contain several hundreds of  
78 individual chemical species, needs to be reduced to a proper surrogate of a few chemical species [15,  
79 16]. Reaction kinetics of the surrogate molecules is consequently developed based on experimental  
80 datasets for the neat substances. Fundamental chemical kinetics experiments on real fuels are scarce  
81 and often limited to global parameters such as ignition delay time e.g. [15, 17] and laminar flame  
82 speed e.g. [18]. For these global parameters jet fuels complying the ASTM specification do not show  
83 distinct differences [19].

84 Resolving species evolution for complex fuels is a challenging task. Investigations are typically  
85 limited to a limited set of technical fuels. Dagaut and coworkers [20] have performed a noticeable  
86 number of speciation experiments in a jet-stirred-reactor for technical fuels e.g. Gas-To-Liquid SPK  
87 [21]. Data are also available from Princeton's variable pressure flow reactor [22] or shock-tube  
88 species-time history measurements [14]. To the best of our knowledge no systematic investigation  
89 of a larger number of technical fuels has been performed on a speciation level. With high regards to  
90 the famous answer to the ultimate question for life, universe, and everything in Douglas Adam's  
91 "The Hitchhiker's Guide to the Galaxy" – 42 – we present a dataset on this number of aviation fuels  
92 in Part-I. This collection was measured under comparable boundary conditions at the DLR high-

93 temperature flow reactor [23] with coupled molecular-beam mass spectrometry (MBMS) for  
94 quantitative speciation of the occurring combustion intermediates.

## 95 **2. Fuels**

96 The 42 fuels investigated in this study cover a broad range of approved SAFs, blend stocks,  
97 candidates for approval, and technical products outside the present ASTM-D7566 specification. The  
98 set is completed by reference fuels (ASTM-D1655), covering a wide range of crude-based jet fuels.  
99 The fuels have been acquired within different international projects, which provide additional data  
100 ranging from generic test rig and burner results up to full size aero engine measurements. Fuels are  
101 shortly described and linked to their projects and additional data available.

102 The Fischer-Tropsch (FT) fuels investigated within the framework of the DLR project “Emission  
103 and Climate Impact of Alternative Fuels” (ECLIF) include the FSJF as well as three different blends  
104 of Semi-Synthetic Jet Fuels (SSJF1-3) provided by the South African FT-specialist SASOL. For  
105 these certified fuels, ground [10] and in-flight [7] exhaust gas measurements have been performed in  
106 the plume of the IAE V2527-A5 engines of DLR’s A320 Advanced Technology Research Aircraft  
107 (DLR-ATRA). The choice of FT-Fuels is completed by six product streams also provided by SASOL  
108 and a crude FT-product (“FT-Light”) from a Power-to-Liquid source [24] extending the database  
109 beyond the limitations of the ASTM specification.

110 Hydroprocessed Esters and Fatty Acids (HEFA) are represented by the fuels used in NASA-DLRs  
111 ACCESS2 (Alternative Fuel Effects on Contrails and Cruise Emissions Study) campaign [6, 25],  
112 namely a 50:50 blend of low sulfur Jet A and HEFA-SPK fuel. Ground and flight measurement  
113 results are available for the CFM56-2-C1 NASA DC-8 aircraft [6]. Three further HEFA (Paramount  
114 Refinery) blends have been studied within the joint “NASA/DLR-Multidisciplinary Airborne  
115 eXperiments” (ND-MAX) or ECLIF2 campaign, where ground and flight measurements with the  
116 DLR-ATRA have been performed. Due to the renewable feedstock the fuels are called “Sustainable  
117 Alternative Jet Fuel” (SAJF1-3). These approved fuel blends have been accompanied by two blends  
118 and a neat High Freezing Point (HFP) HEFA product currently tested by Neste for aviation purposes.

119 Another bio-derived jet fuel investigated here is ARA catalytic hydrothermolysis (CHJ) fuel  
120 (ReadiJet™) obtained from an engine (CFM56-5-C4) exhaust measurement campaign (airegEM) at  
121 an engine test facility [26]. This fuel also fulfills the ASTM specification parameters and was  
122 approved recently. Due to the feedstock we have grouped the CHJ fuel with the HEFA fuels.

123 As a third class, fuels involving biotechnological fermentation of sugar or starch are included.  
124 Among the approved fuels of this group are ATJ and SIP. SIP consists almost exclusively (98%) of  
125 a single molecule: Farnesane (2,6,10-Trimethyldodecane, C<sub>15</sub>H<sub>32</sub>) [27, 28]. The ATJ investigated in  
126 this study also primarily consist of a limited number of molecules: 2,2,4,6,6-pentamethyl heptane  
127 C<sub>12</sub>H<sub>26</sub> (75%) and 2,2,4,4,6,8,8-heptamethyl nonane C<sub>16</sub>H<sub>34</sub> (16%) the remainder are other highly  
128 branched C7-C22 isoparaffins. The neat ATJ was also used for emissions measurement on a CFM56-  
129 5C4 engine [26] at a test rig. Additionally, we have completed the list by looking at ATJ-SKA [29],  
130 which contains an adequate fraction of aromatics to fulfill the final blend specification requirements.  
131 Approval of this fuel type is ongoing.

132 Finally, we have investigated approved fuel blends containing multiple alternative components.  
133 Within the German national framework of “DEMO-SPK” [30] a so-called multiblend (MB)  
134 containing HEFA and ATJ was used for emissions measurement on an A300-600F (Pratt & Whitney  
135 PW4158 engine). Moreover, a multiblend containing additional SIP (MB SIP) was investigated also  
136 herein.

137 For comparison 13 conventional crude-based jet fuels were investigated. These include the reference  
138 fuels used in the above mentioned projects: ECLIF [10], ECLIF2/ND-MAX, ACCESS2 [6], airegEM  
139 [26] and DEMO-SPK [30]. Additionally the fuels POSF-10264 (A1), POSF-10325 (A2) and POSF-  
140 10289 (A3) were gathered from the US consortium “National Jet Fuel Combustion Program”  
141 (NJFCP) [31]. Within the EU-H2020 project JETSCREEN an additional Jet A-1 fuel (JS-A1) and  
142 its severely hydrotreated (JS-A1.3) version have been measured alongside with high naphthalene  
143 containing fuel surrogates (JS-C1 and C3). Table 1 summarizes the investigated fuels, their grouping  
144 as used within the present work and respective literature references. Selected key properties are  
145 summarized in Tab. 2.

146 **Table 1:** Summary of fuel naming and grouping.

#	Fuel	Long name	Group	Reference
1	E1-Ref1	ECLIF Ref 1	Fossil	[10]
2	E1-Ref2	ECLIF Ref 2	Fossil	[10]
3	E1-SSJF1	ECLIF SSJF 1	FT	[10]
4	E1-SSJF2	ECLIF SSJF 2	FT	[10]
5	E1-SSJF3	ECLIF SSJF 3	FT	[10]
6	E1-FSJF	ECLIF FSJF	FT	[10]
7	S-IPK	SASOL IPK	FT	-
8	S-IPK-A	SASOL IPK-A	FT	-
9	S-HN1	SASOL Heavy Naphtha #1	FT	-
10	S-HN2	SASOL Heavy Naphtha #2	FT	-
11	S-LD1	SASOL Light Distillate #1	FT	-
12	S-LD2	SASOL Light Distillate #2	FT	-
13	E2-Ref3	ECLIF2/ND-MAX Ref 3	Fossil	-
14	E2-Ref4	ECLIF2/ND-MAX Ref 4	Fossil	-
15	E2-SAJF1	ECLIF2/ND-MAX SAJF 1	HEFA	-
16	E2-SAJF2	ECLIF2/ND-MAX SAJF 2	HEFA	-
17	E2-SAJF3	ECLIF2/ND-MAX SAJF 3	HEFA	-
18	JS-B2	ECLIF2/ND-MAX HEFA	HEFA	-
19	aEM-Ref	airegEM Ref	Fossil	[26]
20	JS-B3	airegEM ReadiJet™	HEFA	[26]
21	JS-B1	airegEM ATJ	Alc./Sug.	[26]
22	ATJ-SKA	ATJ-SKA	Alc./Sug.	[29]
23	SIP	SIP (Farnesane)	Alc./Sug.	[29]
24	FT-Light	FT-Light	FT	[24]
25	D-Ref-A/C	DEMO-SPK Ref A/C	Fossil	[30]
26	D-Ref-Lab	DEMO-SPK Ref Lab	Fossil	[32]
27	D-MB-A/C	DEMO-SPK MB A/C	HEFA	[30]
28	D-MS-SIP	DEMO-SPK MB SIP	HEFA	[30]
29	JS-A1	JETSCREEN JS-A1	Fossil	[33]
30	JS-A1.3	JETSCREEN JS-A1.3	Fossil	[33]
31	JS-B1	JETSCREEN JS-B1	Alc./Sug.	[33]
32	JS-C1	JETSCREEN JS-C1	-	[33]
33	JS-C3	JETSCREEN JS-C3	-	[33]
34	NJFCP-A1	NJFCP A1 (JP-8 POSF 10264)	Fossil	[31]
35	NJFCP-A2	NJFCP A2 (Jet-A POSF 10325)	Fossil	[31]
36	NJFCP-A3	NJFCP A3 (JP-5 POSF 10289)	Fossil	[31]
37	Acc-Ref	ACCESS2 Reference	Fossil	[6]
38	Acc-HEFA50	ACCESS2 HEFA Blend (50:50)	HEFA	[6]
39	N-Ref	Neste Jet A-1 Ref	Fossil	-
40	N-HFP-B1	Neste HFP HEFA Blend 1	HEFA	-
41	N-HFP-B2	Neste HFP HEFA Blend 2	HEFA	-
42	N-NeatHFP	Neste HFP HEFA Neat	HEAF	-

**Table 2:** Summary of selected fuel properties.

Fuel	wH (NMR) <sup>a</sup> [mass-%]	IHD <sup>b</sup> [-]	wNa <sup>c</sup> [mass-%]	M (L&K) <sup>d</sup> [g/mol]	wH (GCxGC) [mass-%]	M (GCxGC) [g/mol]	n/iso-Par. ratio [-]	n- Paraffins [mass-%]	iso- Paraffins [mass-%]	mono- cyclic Paraffins [mass-%]	bicyclic Paraffins [mass-%]	poly- cyclic Paraffins [mass-%]	mono- cyclic Aromatics [mass-%]	mono- cyclic Aromatics [mass-%]	mono- cyclic Aromatics [mass-%]	GCxGC Source
E1-Ref1	13.67	1.460	1.78	166	13.9	155	0.947	22.2	23.4	23.2	9.3	1.5	13.5	4.5	2.4	<sup>e</sup>
E1-Ref2	13.73	1.451	2.29	165	13.9	155	1.171	25.4	21.7	22.6	8.8	1.3	13.3	3.7	3.2	<sup>e</sup>
E1-SSJF1	14.36	0.851	1.04	162	14.5	158	0.259	14.0	54.0	14.5	5.2	0.8	7.8	2.4	1.4	<sup>e</sup>
E1-SSJF2	14.53	0.763	0.99	156	14.6	156	0.193	11.8	61.0	11.8	4.4	0.4	7.5	1.7	1.4	<sup>e</sup>
E1-SSFJ3	14.01	1.277	1.52	164	14.1	156	0.625	20.2	32.3	20.5	7.9	1.3	11.7	4.0	2.1	<sup>e</sup>
E1-FSJF	14.17	1.113	0.30	159	14.3	160	0.074	3.7	49.7	13.1	16.4	7.7	3.7	5.4	0.2	<sup>e</sup>
S-IPK	15.34	0.048	0.01	152	15.4	158	0.000	0.0	95.2	4.8	0.0	0.0	0.0	0.0	0.0	<sup>e</sup>
S-IPK-A	14.31	1.022	0.01	155	14.3	156	0.031	2.2	68.7	7.2	1.0	0.0	20.4	0.6	0.0	<sup>e</sup>
S-HN1	14.79	0.616	0.02	147	14.8	140	1.453	45.4	31.2	9.5	5.7	0.0	5.0	3.1	0.0	<sup>e</sup>
S-HN2	12.57	2.367	0.40	139	12.6	130	2.107	22.6	10.7	12.3	9.4	0.0	35.0	9.7	0.3	<sup>e</sup>
S-LD1	14.01	1.240	0.27	180	14.1	166	1.046	31.7	30.3	12.6	2.1	0.1	16.3	6.4	0.2	<sup>e</sup>
S-LD2	12.87	2.379	0.67	179	12.9	167	1.946	5.5	2.8	17.6	38.9	15.3	4.5	14.8	0.5	<sup>e</sup>
E2-Ref3	13.65	1.624	1.67	165	13.7	152	0.760	15.3	20.1	28.6	13.5	0.7	12.3	7.6	2.0	<sup>e</sup>
E2-Ref4	14.08	1.251	0.11	152	14.1	143	0.917	22.1	24.1	28.0	7.5	0.1	14.2	4.0	0.2	<sup>e</sup>
E2-SAJF1	14.40	0.903	0.86	169	14.5	156	0.344	16.8	48.8	14.9	7.2	0.3	6.7	4.1	1.1	<sup>e</sup>
E2-SAJF2	14.51	0.891	0.06	156	14.5	146	0.560	22.4	40.1	20.3	4.4	0.1	9.9	2.7	0.1	<sup>e</sup>
E2-SAJF3	14.04	1.255	0.92	162	14.1	150	0.591	18.3	31.0	24.0	9.2	0.4	10.7	5.4	1.1	<sup>e</sup>
JS-B2	15.37	0.022	0.01	172	15.4	166	0.205	16.8	81.8	1.2	0.1	0.0	0.1	0.0	0.0	<sup>e</sup>
aEM-Ref	13.98	1.374	1.66	165	n/a	n/a	n/a	n/a	n/a	n/a	n/a	n/a	n/a	n/a	n/a	n/a
JS-B3	13.60	1.834	0.22	165	13.5	159	1.864	17.5	9.4	30.6	17.3	0.0	14.4	10.5	0.3	<sup>f</sup>
JS-B1	15.31	0.001	0.00	160	15.3	180	0.000	0.0	99.9	0.1	0.0	0.0	0.0	0.0	0.0	<sup>f</sup>
ATJ-SKA	14.61	0.780	0.04	146	n/a	n/a	n/a	n/a	n/a	n/a	n/a	n/a	n/a	n/a	n/a	n/a
SIP	15.09	0.000	0.00	204	15.2	212	0.000	n/a	n/a	n/a	n/a	n/a	n/a	n/a	n/a	n/a
FT-Light	15.12	0.266	0.01	152	15.2	140	60.377	71.5	1.2	23.8	0.0	0.0	0.0	0.0	0.0	[24]
D-Ref-A/C	13.79	1.535	0.33	158	n/a	n/a	n/a	n/a	n/a	n/a	n/a	n/a	n/a	n/a	n/a	n/a
D-Ref-Lab	13.93	1.424	0.28	158	n/a	n/a	n/a	n/a	n/a	n/a	n/a	n/a	n/a	n/a	n/a	n/a
D-MB-A/C	14.32	1.049	0.25	160	n/a	n/a	n/a	n/a	n/a	n/a	n/a	n/a	n/a	n/a	n/a	n/a

Fuel	wH (NMR) <sup>a</sup> [mass-%]	IHD <sup>b</sup> [-]	wNa <sup>c</sup> [mass-%]	M (L&K) <sup>d</sup> [g/mol]	wH (GCxGC) [mass-%]	M (GCxGC) [g/mol]	n/iso-Par. ratio [-]	n-Paraffins [mass-%]	iso-Paraffins [mass-%]	mono-cyclic Paraffins [mass-%]	bicyclic Paraffins [mass-%]	poly-cyclic Paraffins [mass-%]	mono-cyclic Aromatics [mass-%]	mono-cyclic Aromatics [mass-%]	mono-cyclic Aromatics [mass-%]	GCxGC Source
D-MS-SIP	14.14	1.225	0.23	166	n/a	n/a	n/a	n/a	n/a	n/a	n/a	n/a	n/a	n/a	n/a	n/a
JS-A1	14.02	1.341	1.36	156	14.0	150	0.625	19.2	30.7	21.8	8.0	0.0	15.5	2.9	1.8	f
JS-A1.3	14.43	0.886	0.03	156	14.5	150	0.622	20.6	33.1	26.5	10.7	0.0	8.0	1.0	0.0	f
JS-B1	15.31	0.001	0.00	155	15.3	180	0.000	0.0	99.9	0.1	0.0	0.0	0.0	0.0	0.0	f
JS-C1	12.66	2.859	14.58	190	12.6	182	0.673	10.1	15.0	16.4	25.7	8.1	1.9	2.9	19.9	f
JS-C3	13.68	1.781	4.72	195	13.1	185	0.669	12.2	18.2	17.3	26.1	8.0	2.5	2.3	13.4	f
NJFCP-A1	14.37	0.923	0.86	159	14.5	152	0.676	26.9	39.7	17.0	3.0	0.1	10.9	1.5	1.1	[31]
NJFCP-A2	13.90	1.363	2.12	168	14.0	159	0.680	20.1	29.5	24.9	6.8	0.2	12.9	3.4	2.3	[31]
NJFCP-A3	13.56	1.746	1.06	175	13.6	166	0.766	13.9	18.2	31.4	16.0	0.1	10.4	8.9	1.3	[31]
Acc-Ref	13.70	1.656	0.94	168	n/a	n/a	n/a	n/a	n/a	n/a	n/a	n/a	n/a	n/a	n/a	n/a
Acc-HEFA50	14.42	0.948	0.48	172	n/a	n/a	n/a	n/a	n/a	n/a	n/a	n/a	n/a	n/a	n/a	n/a
N-Ref	13.99	1.325	0.56	147	n/a	n/a	n/a	n/a	n/a	n/a	n/a	n/a	n/a	n/a	n/a	n/a
N-HFP-B1	14.16	1.184	0.45	151	n/a	n/a	n/a	n/a	n/a	n/a	n/a	n/a	n/a	n/a	n/a	n/a
N-HFP-B2	14.31	1.059	0.40	160	n/a	n/a	n/a	n/a	n/a	n/a	n/a	n/a	n/a	n/a	n/a	n/a
N-NeatHFP	15.04	0.090	0.03	235	n/a	n/a	n/a	n/a	n/a	n/a	n/a	n/a	n/a	n/a	n/a	n/a

<sup>a</sup> Hydrogen content measured according to ASTM-D7171

<sup>b</sup> Index of Hydrogen Deficiency calculated according to Eq.1

<sup>c</sup> Naphthalene content measured according to ASTM-D1840, Limit of quantification LoQ=0.1 mass-%

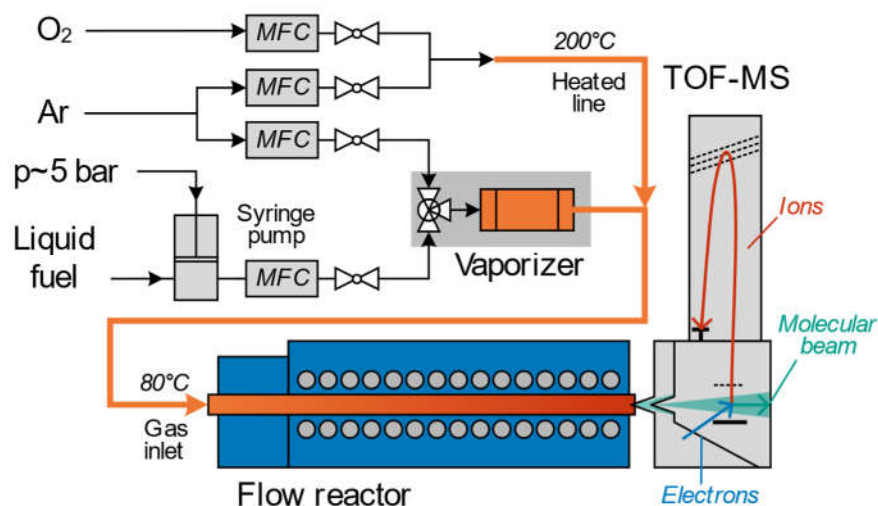
<sup>d</sup> Lee Kesler [34] correlation between T50, density and molar mass

<sup>e</sup> GCxGC-Source: Sasol Energy, South Africa

<sup>f</sup> GCxGC-Source: IFP Energies Nouvelles (IFPEN), France

150 **3. Experiment**

151 The experimental approach follows previous studies [35-38]. Thus only a brief description is  
152 presented here with more details available in [23] including a detailed description of the experimental  
153 set-up and data evaluation. A schematic drawing is given in Fig. 1.



154  
155 **Figure 1:** Experimental set-up: Flow reactor with time-of-flight mass spectrometer (TOF-MS) and gas supply  
156 including Coriolis mass flow controller (MFC).

157 The DLR high-temperature flow reactor consists of a reactor including gas supply, and the coupled  
158 molecular beam mass spectrometry (MBMS) system for detection of the reaction intermediates. The  
159 reactor (40mm diameter, 1000mm heated length) is placed in a high-temperature oven operating at  
160 ambient pressure (~980mbar). Highly diluted reactants (oxygen, pre-vaporized fuel, 99% Ar) are fed  
161 to the reactor at moderate temperatures (80°C). Mass flows are controlled using Coriolis flow meters  
162 for high precision, particularly useful for the chemically complex technical fuel mixture. The fuel is  
163 completely evaporated (Bronkhorst CEM) and supplied slightly heated into the reactor. Complete  
164 evaporation is ensured (and controlled regularly) by the low fuel fraction requiring only a low vapor  
165 pressure.

166 All measurements are designed to keep the carbon and diluent flow constant throughout the  
167 experiments. For all fuels, slightly rich ( $\Phi=1.2$ ) and lean ( $\Phi=0.8$ ) conditions are achieved by adding  
168 the respective amounts of oxygen which may consequently lead to slightly differed total volume

169 flow. The resulting difference in residence time is, however, negligible due to the high dilution. Inlet  
170 conditions are summarized in Table 3. Stoichiometry  $\Phi$  is calculated from the NMR (ASTM-D7171)  
171 results for Hydrogen content. Heteroatoms are neglected. Measurements are performed by applying  
172 a constant-rate decreasing temperature ramp (-200K/h) covering the full range of complete oxidation  
173 to the unburnt reactants (typically 750-1200 K). Resulting residence times are in the range of 2s  
174 depending on the respective oven temperature.

175 Chemical species exiting the reactor are quantitatively monitored with the MBMS system by  
176 quenching the reaction immediately through rapid expansion into a molecular beam. The molecular  
177 beam is guided through the electron ionization (EI) ion source of the TOF mass spectrometer, which  
178 is capable of resolving the elemental composition (C/H/O) of the occurring stable and reactive  
179 combustion intermediates. Soft ionization conditions (10.5eV, actual value) are applied to avoid  
180 fragmentation of the species at the ion source.

181 Major species (reactants and products) are recorded in parallel by a quadrupole MS operating at high  
182 ionization energies (70eV) for optimal sensitivity. Within the quadrupole measurements the m/z 57  
183 signal is recorded and used as average fuel signal. This signal refers to most hydrocarbon species  
184 especially those of aliphatic nature and was used to calculate an average “fuel” profile.

185 Data reduction follows established procedures [23, 37]. Combustion intermediates are calibrated  
186 using cold gas samples of known concentration with a few exceptions where estimation of the  
187 respective ionization cross section based on the RICS method (Relative Ionization Cross Section [23,  
188 39]) was applied. The complex chemical nature of the technical fuels is accounted by calibrating the  
189 fuel compounds according to the detailed GCxGC analysis of the respective fuel when available  
190 (compare Tab. 2). The detailed composition, i.e. mass fractions by chemical class and carbon  
191 number, of the fuels is given in the electronic supplement when available.

192 The experimental uncertainty of the determined mole fractions is typically within  $\pm 20\%$  for direct  
193 calibrated species. Due to the soft ionization, chemical structures of the combustion intermediates  
194 are not resolved and always the sum of isomers is measured. Since individual isomers exhibit

195 individual ionization cross sections, the uncertainty may be significantly higher, when several  
196 isomers occur. Calibration is always based on a single isomer chosen on the basis of experiences  
197 from isomer resolving experiments, e.g. [40, 41]. However, the reproducibility of the experiment is  
198 excellent and relative comparisons between the fuels can be performed with high accuracy. The neat  
199 ATJ fuel (same batch) for instance was measured twice (within the projects JETSCREEN “JS-B1”  
200 and airegEM “ATJ”) by different operators within a time span of about two years. Both  
201 measurements are reported herein and exhibit excellent agreement even though experimental  
202 conditions differ slightly. The full dataset is available from the authors upon request.

203

204 **Table 3:** Inlet flow conditions for the individual measurements. Stoichiometry  $\Phi$  is calculated from the NMR  
 205 (ASTM-D7171) results for Hydrogen content. Heteroatoms are neglected.

Fuel	Ar	Fuel	O <sub>2</sub> (Fuel-rich)		O <sub>2</sub> (Fuel-lean)	
	[g/min]	[mg/min]	[mg/min]	$\Phi$	[mg/min]	$\Phi$
ECLIF Ref 1	17.64	31.1	88.1	1.19	132.1	0.80
ECLIF Ref 2	17.64	31.1	88.1	1.20	132.1	0.80
ECLIF SSJF 1	17.64	31.4	89.7	1.20	134.5	0.80
ECLIF SSJF 2	17.64	31.4	89.9	1.20	134.8	0.80
ECLIF SSJF 3	17.64	31.2	88.5	1.20	132.8	0.80
ECLIF FSJF	17.64	31.3	88.9	1.20	133.4	0.80
SASOL IPK	17.64	31.67	91.77	1.20	137.65	0.80
SASOL IPK-A	17.64	31.3	89.2	1.20	133.8	0.80
SASOL Heavy Naphtha #1	17.64	31.5	90.4	1.20	135.6	0.80
SASOL Heavy Naphtha #2	17.64	30.7	84.94	1.20	127.4	0.80
SASOL Light Distillate #1	17.64	31.1	88.6	1.19	132.9	0.80
SASOL Light Distillate #2	17.64	30.78	85.83	1.20	128.74	0.80
ECLIF2/ND-MAX Ref 3	17.64	31.02	87.5	1.20	131.2	0.80
ECLIF2/ND-MAX Ref 4	17.64	31.19	88.6	1.20	132.9	0.80
ECLIF2/ND-MAX SAJF 1	17.64	31.3	89.3	1.20	133.9	0.80
ECLIF2/ND-MAX SAJF 2	17.64	31.34	89.6	1.20	134.4	0.80
ECLIF2/ND-MAX SAJF 3	17.64	31.17	88.4	1.20	132.6	0.80
ECLIF2/ND-MAX HEFA (JS-B2)	17.64	31.66	91.7	1.20	137.5	0.80
airegEM Ref	17.64	31.2	88.6	1.20	132.9	0.80
airegEM ReadiJet™ (JS-B3)	17.64	31.1	87.7	1.20	131.5	0.80
airegEM ATJ (JS-B1)	17.64	31.7	92.1	1.19	138.2	0.80
ATJ-SKA	17.64	31.5	90.4	1.20	135.7	0.80
SIP (Farnesane)	17.64	31.6	91.2	1.20	136.8	0.80
FT-Light	17.64	31.7	92.0	1.19	138.0	0.80
DEMO-SPK Ref A/C	17.64	31.08	87.8	1.20	131.7	0.80
DEMO-SPK Ref Lab	17.64	31.13	88.1	1.20	132.2	0.80
DEMO-SPK MB A/C	17.64	31.27	89.1	1.20	133.6	0.80
DEMO-SPK MB SIP	17.64	31.2	88.7	1.20	133.0	0.80
JETSCREEN JS-A1	17.64	31.16	88.4	1.20	132.6	0.80
JETSCREEN JS-A1.3	17.64	31.31	89.4	1.20	134.0	0.80
JETSCREEN JS-B1	17.64	31.62	91.4	1.20	137.1	0.80
JETSCREEN JS-C1	17.64	30.69	85.2	1.20	127.9	0.80
JETSCREEN JS-C3	17.64	31.0	87.6	1.20	131.3	0.80
NJFCP A1 (JP-8: POSF 10264)	17.64	31.3	89.2	1.20	133.8	0.80
NJFCP A2 (Jet A: POSF 10325)	17.64	31.1	88.1	1.20	132.1	0.80
NJFCP A3 (JP 5: POSF 10289)	17.64	31.0	87.3	1.20	130.9	0.80
ACCESS2 Reference	17.64	31.1	87.9	1.20	131.8	0.80
ACCESS2 HEFA Blend (50:50)	17.64	31.4	90.0	1.19	135.0	0.80
Neste Jet A-1 Ref	17.64	31.3	89.0	1.20	133.5	0.80
Neste HFP HEFA Blend 1	17.64	31.3	89.5	1.19	134.2	0.80
Neste HFP HEFA Blend 2	17.64	31.4	89.8	1.20	134.7	0.80
Neste HFP HEFA Neat	17.64	31.6	91.5	1.19	137.2	0.80

## 4. Results

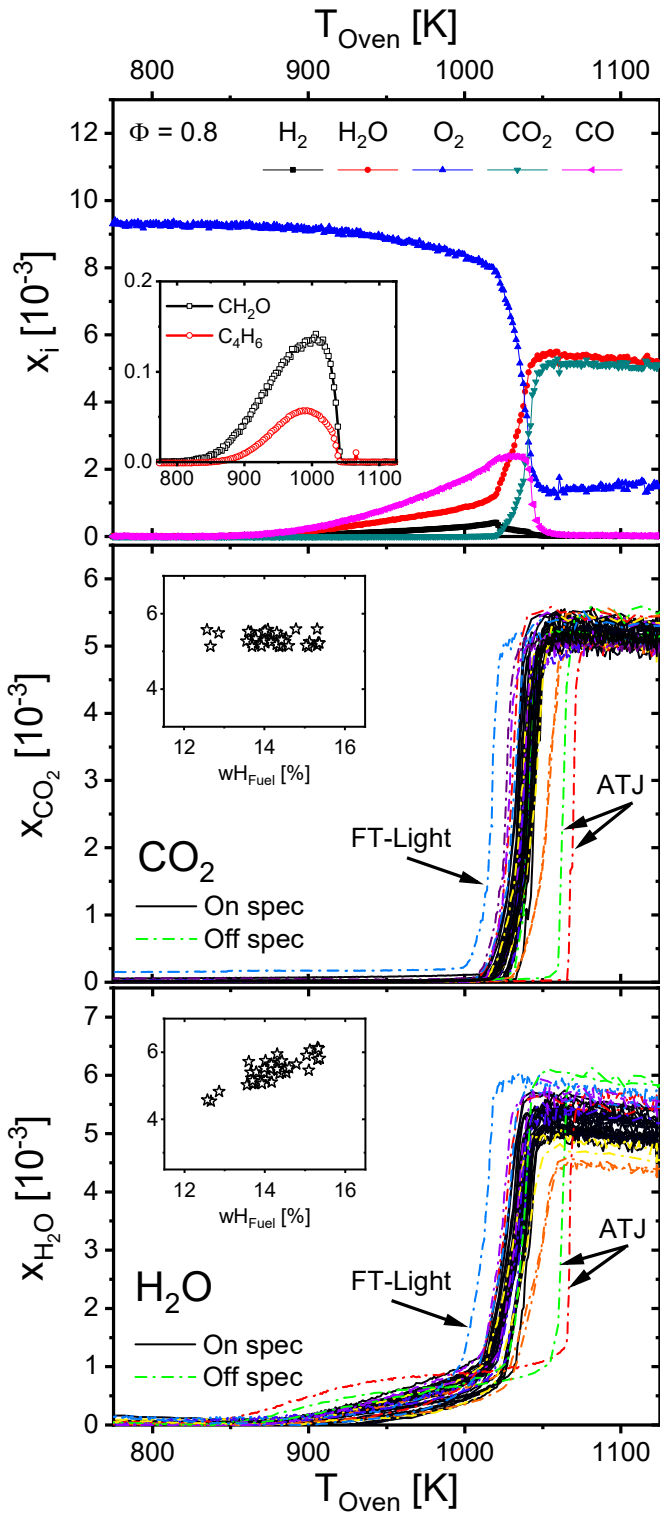
In the following the emphasis are given on the description and interpretation on the experimental results for the 42 jet fuels. Phenomenological findings and relations with the complex fuel composition are presented and discussed. A deep analysis of the underlying chemical reaction network is, however, beyond the scope of the present publication. The interested reader is referred to Part-II [42] and Part-III [43] of this series for further insights.

### 4.1 Fuel Decay and Major Species

The global reaction behavior of the 42 technical fuels, i.e. concentration profiles of the reactants and products, follows the expectations as drawn from single compound fuels [37, 44]. Figure 2 gives an example of the major species profile evolution for the multiblend containing conventional and three alternative fuel components (DEMO-SPK MB SIP) at lean conditions. At low reactor temperatures the reactants pass the reactor unaltered. With increasing temperature fuel decay and conversion into first combustion intermediates, e.g. formaldehyde ( $\text{CH}_2\text{O}$ ) and butadiene ( $\text{C}_4\text{H}_6$ ), can be observed (compare insert). Simultaneously, a slight consumption of oxygen as well as formation of hydrogen and carbon monoxide occurs. Evolution of the species pool towards smaller intermediates can be observed with increasing reactor temperature (not shown). At a certain temperature, rapid conversion is observed when radical producing chain branching reactions overshoot the chain termination reactions. A steep increase of the final products  $\text{H}_2\text{O}$  and  $\text{CO}_2$  is observed with complete intermediate consumption. The reactor temperature can be interpreted as a kind of reaction progress variable. Due to the well-characterized temperature conditions in the reactor, detailed kinetic modeling is feasible and has been previously demonstrated for single species fuels, e.g. methane [38], ethylene glycol [45] or n-alkanes [44]. The detailed examination of the reaction network of the complex fuels considered here is possible based on the presented data and is presented in Part-III of the present series [43]. The aim of this part is to analyze the differences observed in the intermediate species pool of this large set of fuels in the following.

232 The product profiles for water and carbon dioxide of all fuels are compared in Fig. 2. Intentionally,  
233 the final concentration of CO<sub>2</sub> is similar for all fuels, since the reaction conditions are designed to  
234 exhibit similar carbon flows. Once conversion is complete the CO<sub>2</sub> concentrations are identical for  
235 all fuels, as shown for the lean conditions presented. Additionally, the experimental accuracy can be  
236 read from the deviation of the measured values and is found to be well within 10%. Consistently, the  
237 H<sub>2</sub>O concentration for a specific fuel depends on the hydrogen content of that fuel.

238 The temperature for full occurrence of conversion is of interest, and can be visualized by both species  
239 (CO<sub>2</sub> and H<sub>2</sub>O). All fuels that fulfill the ASTM specification requirements exhibit very similar  
240 profiles with a span of only 8K, which is below to the temperature accuracy of the experiment  
241 ( $\pm 10$ K). This observation indicates similar reaction properties, i.e. ignition delay time and flame  
242 speed, which is consistent with previous findings [19] and a key intention of the standardization of  
243 fuel properties. Noticeable differences only occur for fuels that are clearly outside the specification  
244 requirements, such as for the FT-crude (FT-Light) product (lowest temperature) and the ATJ (highest  
245 temperature). The FT-Light almost exclusively consists of n-alkanes, while the major constituent of  
246 the ATJ fuel are two highly branched alkanes containing tertiary carbons similar to iso-octane. The  
247 resulting tert-butyl radicals produced by the ATJ are inert compared to other hydrocarbon radicals  
248 and thus exhibits delayed ignition as known from the octane index for spark ignition engine fuels.  
249 Furthermore, it should be noted that the ATJ exhibits slightly staged profile shapes for H<sub>2</sub>O and O<sub>2</sub>  
250 as observed for iso-octane [42]. The interested reader is referred to Part-II of this series for a detailed  
251 examination of the reaction network of linear and branched alkanes [42] including the present fuels.



252

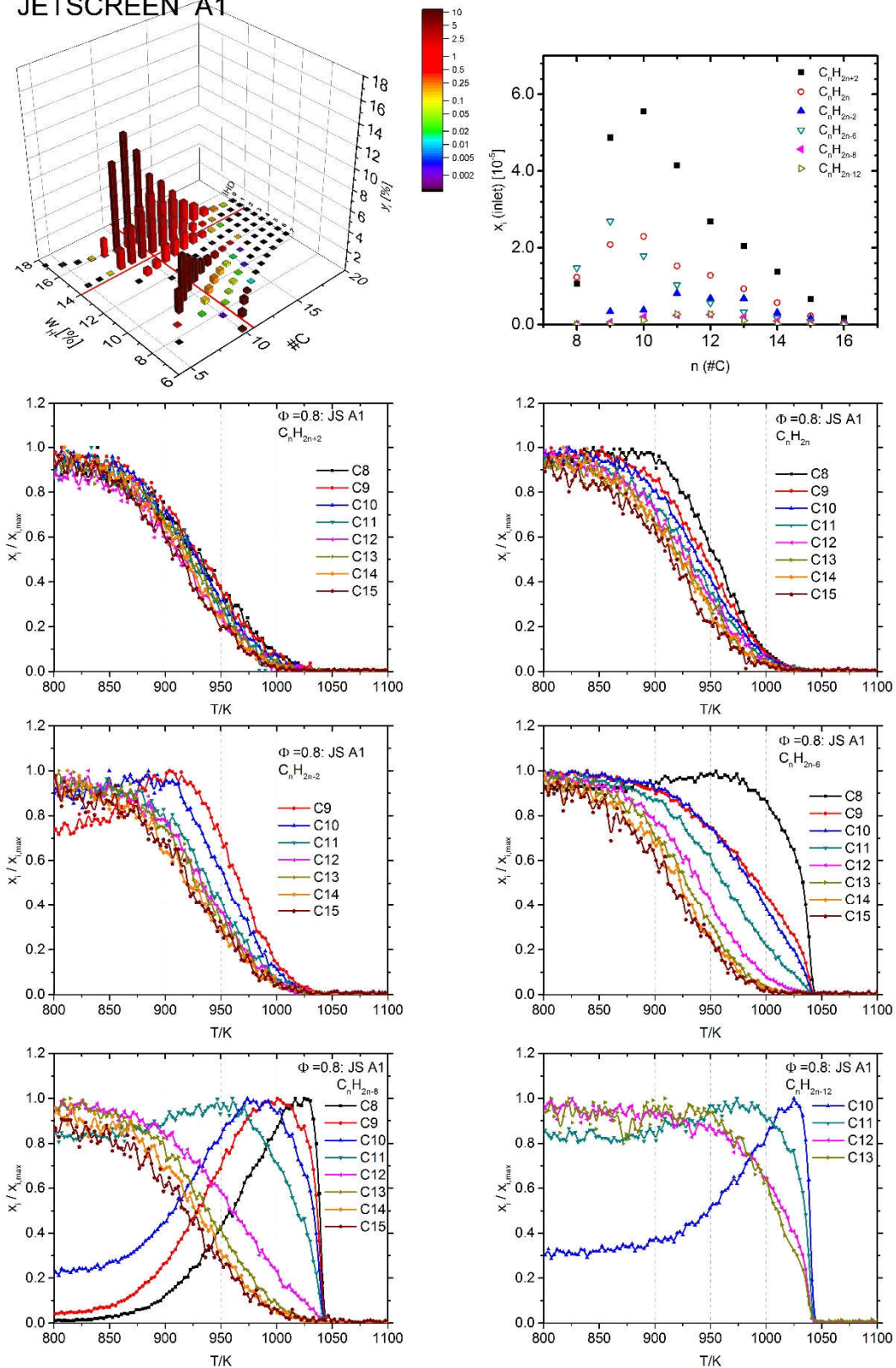
253 **Figure 2:** Major species and representative intermediates (CH<sub>2</sub>O and C<sub>4</sub>H<sub>6</sub>) for the “Multiblend” kerosene  
 254 containing HEFA, ATJ, SIP and conventional kerosene (panel 1). Comparison of carbon dioxide (panel 2) and  
 255 water profiles (panel 3) for all fuels ( $\Phi=0.8$ ). Fuels outside the ASTM-D7566 specification are drawn in dashed  
 256 lines. Inserts show the respective maximum values as function of the fuels’ hydrogen content.

257

258 The present experiment allows for species resolved observation of the individual fuel molecules  
259 destruction during the oxidation reaction. The decay behavior depends in general more on the  
260 individual chemical classes than on the particular fuel. Since most of the fuels presented here are  
261 mixtures containing several hundreds of chemical species, a detailed quantitative determination is  
262 barely possible by the TOF-MBMS. When detailed fuel composition (see electronic supplement) is  
263 available then, the fuel profiles are calibrated accordingly. Figure 3 gives the species profiles by  
264 chemical class for the Jetscreen “JS A1” fuel as example, for comparison profiles are normalized to  
265 their respective maximum. Jetscreen “JS A1” represents a regular fossil Jet A-1 fuel exhibiting a  
266 composition close to the “world average” as determined in ref. [46]. Similar plots are given in the  
267 electronic supplement for each of the fuels.

268 As a rough generalization the decay order, i.e. the temperature at which a class starts to be consumed,  
269 can be stated in accordance to the thermal stability: n/iso-alkanes < cycloalkanes < mono-aromatics  
270 < di-aromatics. Additionally, a dependence on the chain length, i.e. carbon number, can be stated  
271 within some chemical classes. In particular only minor differences can be observed for the decay  
272 behavior of n- and iso-paraffins while a small shift towards lower decay temperatures can be stated  
273 for cyclic (mono- and di-) paraffins. Within in these classes some small species (e.g. C<sub>8</sub>H<sub>16</sub> or C<sub>9</sub>H<sub>16</sub>)  
274 are even formed in small amounts as intermediate by the chemical reactions prior beginning of their  
275 consumption. Classes containing aromatic structures (mono-, naphtheno- or diaromatics) in general  
276 show a distinct dependence on the respective chain length. Among these classes also typical  
277 combustion and soot precursor intermediates can be found. Indeed, a typical intermediate species  
278 profile is seen for the smaller molecules of the aromatic classes. The transition from “intermediate”  
279 to “fuel” profile shape occurs at C<sub>9</sub> for monoaromatics, C<sub>11</sub> for naphthenoaromatics and C<sub>12</sub> for  
280 diaromatics. The occurrence of an intermediate species behavior is found to be highly dependent on  
281 the specie’s initial concentration at the respective fuel. In general, the fuel decay profiles are found  
282 to be quite similar for all fuels as long as the respective class is a constituent of the fuel.

### JETSCREEN A1



283

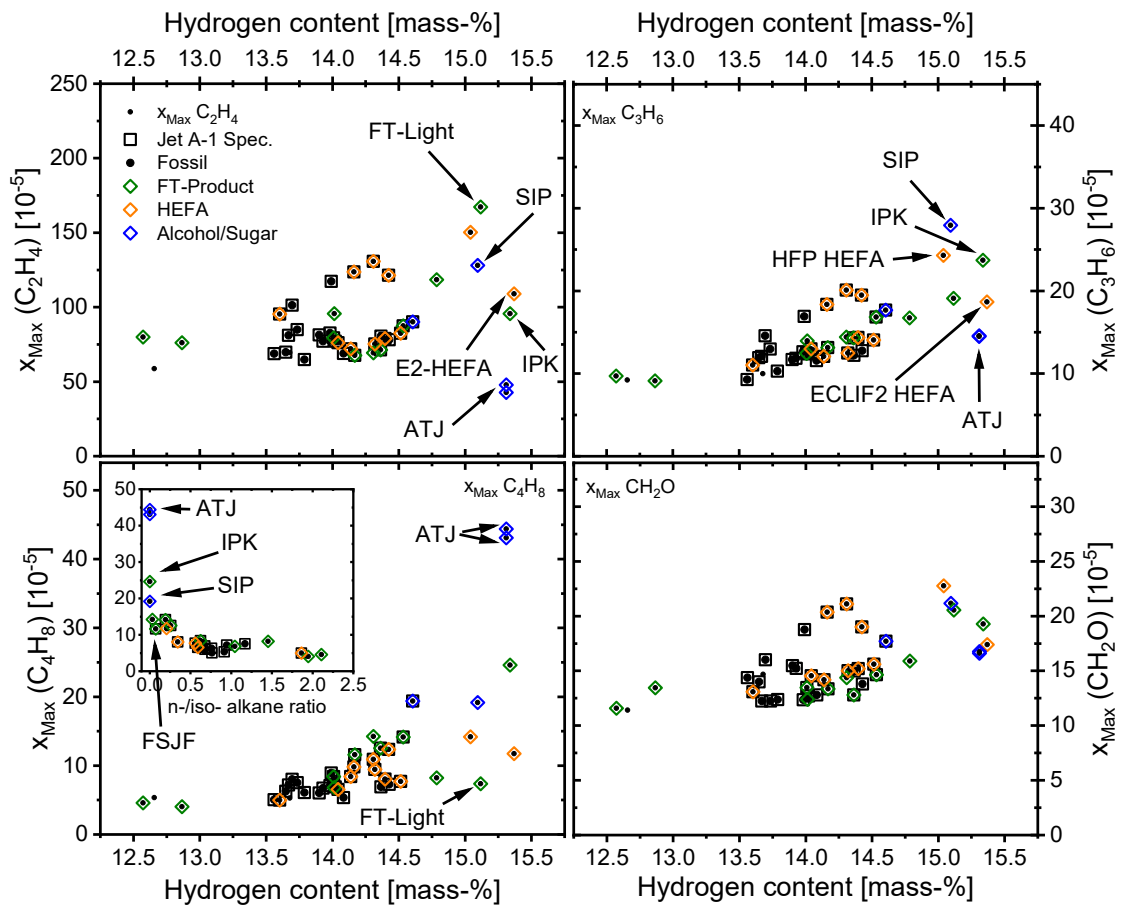
284 **Figure 3:** Fuel composition for Jetscreen JS A1 (top, left) and respective inlet mole fractions (top, right). Lower  
 285 panels show the normalized fuel species profiles for the respective chemical class: n/iso-paraffins ( $C_nH_{2n+2}$ ),  
 286 mono-cyclic paraffins ( $C_nH_{2n}$ ), bicyclic paraffins ( $C_nH_{2n-2}$ ), mono-cyclic aromatics ( $C_nH_{2n-6}$ ), naphthenic-  
 287 mono-aromatics ( $C_nH_{2n-8}$ ), diaromatics ( $C_nH_{2n-12}$ ).

## 288 4.2 Small Intermediate Species

289 In the following sections intermediate species concentrations are compared for the different fuels.  
290 Since the profile shapes and peak temperatures are quite similar, we will focus on the measured peak  
291 mole fractions only. Figure 4 summarizes some important combustion intermediates: ethylene  
292 ( $C_2H_4$ ), propene ( $C_3H_6$ ), butene ( $C_4H_8$ ), and formaldehyde ( $CH_2O$ ). Peak mole fractions are plotted  
293 against the fuel's hydrogen content since many combustion properties are linked to this fuel property.  
294 Ethylene as most other small combustion intermediates does not show a distinct relation with the  
295 fuel hydrogen content. Most fuels exhibit even similar peak concentrations ( $x(C_2H_4) \sim 7.5 \cdot 10^{-6}$ ). It is  
296 noticeable that hydrogen-rich fuels depart significantly from the mean value. For these neat aliphatic  
297 fuels, a strong influence of the fuel structure is observed: the highest amount of  $C_2H_4$  is seen for the  
298 n-alkane rich FT-Light fuel while the lowest is seen for the highly branched ATJ (major constituents:  
299 2,2,4,6,6-pentamethyl heptane and 2,2,4,4,6,8,8-heptamethyl nonane).

300 The influence of the branching structure of alkanes can also be stated for propene ( $C_3H_6$ ). Here the  
301 slightly branched farnesane exhibits the highest concentration. This finding agrees well with the  
302 decomposition pathways of this molecule [37] that provides many pathways towards propene and  
303 other C3-intermediates. The FT crude fuel (FT-Light) and a HEFA exhibits a mean value, and ATJ  
304 again shows a relatively low mole fraction. In contrast to  $C_2H_4$  a slight increase of the  $C_3H_6$  peak  
305 concentrations can be stated with increasing hydrogen content of the fuel. The butene ( $C_4H_8$ ) peak  
306 maxima exhibit a clear dependence on the hydrogen content. The divergence between the fuels is  
307 higher for the aliphatic fuels. For butene a clear dependence on the molecular structure is seen. Values  
308 are additionally plotted versus n/iso-alkane ratio of the fuel. Highest values are seen for ATJ followed  
309 by a commercial SPK (SASOL IPK) and farnesane (SIP), all of which do not contain any n-alkanes.  
310 In combination, the amount and branching ratios of the alkanes dominate the  $C_4H_8$  peak mole  
311 fraction. It should be noted that no separation of 1-, 2- and isobutene was obtained here, and the split  
312 between these isomers will also be highly dependent on the fuel structure and also may influence the  
313 accuracy of the measured peak mole fractions. Oxygenated intermediates, formaldehyde ( $CH_2O$ ) for

314 instance, show only a slight dependence on the fuel hydrogen content but no distinct relation to the  
 315 molecular fuel structure can be drawn.



316

317 **Figure 4:** Peak mole fraction ( $\Phi=0.8$ ) of the combustion intermediates ethylene ( $C_2H_4$ ), propylene ( $C_3H_6$ ),  
 318 butene ( $C_4H_8$ ) and formaldehyde ( $CH_2O$ ) as a function of the fuel hydrogen content and n-/iso alkane ratio  
 319 (insert). Fuels fulfilling ASTM requirements are highlighted by black squares, colors indicate the respective  
 320 group according Tab. 1.

### 321 4.3 Soot Precursor

322 Soot emission of aero engines was found to correlate with the aromatic content or the hydrogen  
 323 content of the fuel, e.g. [4, 10, 26]. Often both properties are used synonymously since aromatics  
 324 constitutionally exhibit lower hydrogen content than aliphatic species. However, most recent work  
 325 proves the hydrogen content being a better indicator [5, 10]. From single compound fuels it is known  
 326 that the sooting tendency of the chemical classes present in technical jet fuels roughly increase in the  
 327 following order: n-alkanes < iso-alkanes < cycloalkanes (naphthenes) << mono-aromatics < di-  
 328 aromatics [47]. The hydrogen content enables to account for the different structural features to a

329 certain extent. Furthermore, the molecule size is also considered since aliphatic substituents will  
 330 increase the hydrogen content of a molecule. Compare benzene ( $w_H=7.7\text{mass-}\%$ ) vs. dipropyl  
 331 benzene ( $w_H=11.2\text{mass-}\%$ ) for instance. Both molecules exhibit a single aromatic ring and would  
 332 count equally to the aromatics content of the fuel. In the following we further modify this approach  
 333 and use the Index of Hydrogen Deficiency (IHD) [48] of the respective fuel. The IHD accounts for  
 334 the amount of unsaturation in, i.e. number of double bond equivalents of a molecule. Alkenes or  
 335 cycloalkanes for instance exhibit an IHD of one since they have one  $\text{H}_2$  unit less than their respective  
 336 alkane. An aromatic ring consequently yields to an IHD of four. For a complex hydrocarbon fuel  
 337 ( $\text{C}_x\text{H}_y$ ) the IHD is derived according to Eq. 1 based on hydrogen mass fraction ( $w_H$ ) and mean molar  
 338 mass ( $M_{\text{Fuel}}$ ):

$$339 \quad \text{IHD}(\text{C}_x\text{H}_y) = (x + 1) - \frac{y}{2} = \frac{\bar{M}_{\text{Fuel}}(1-w_H)}{M_C} - \frac{w_H \bar{M}_{\text{Fuel}}}{2M_H} + 1 \quad (\text{Eq.1})$$

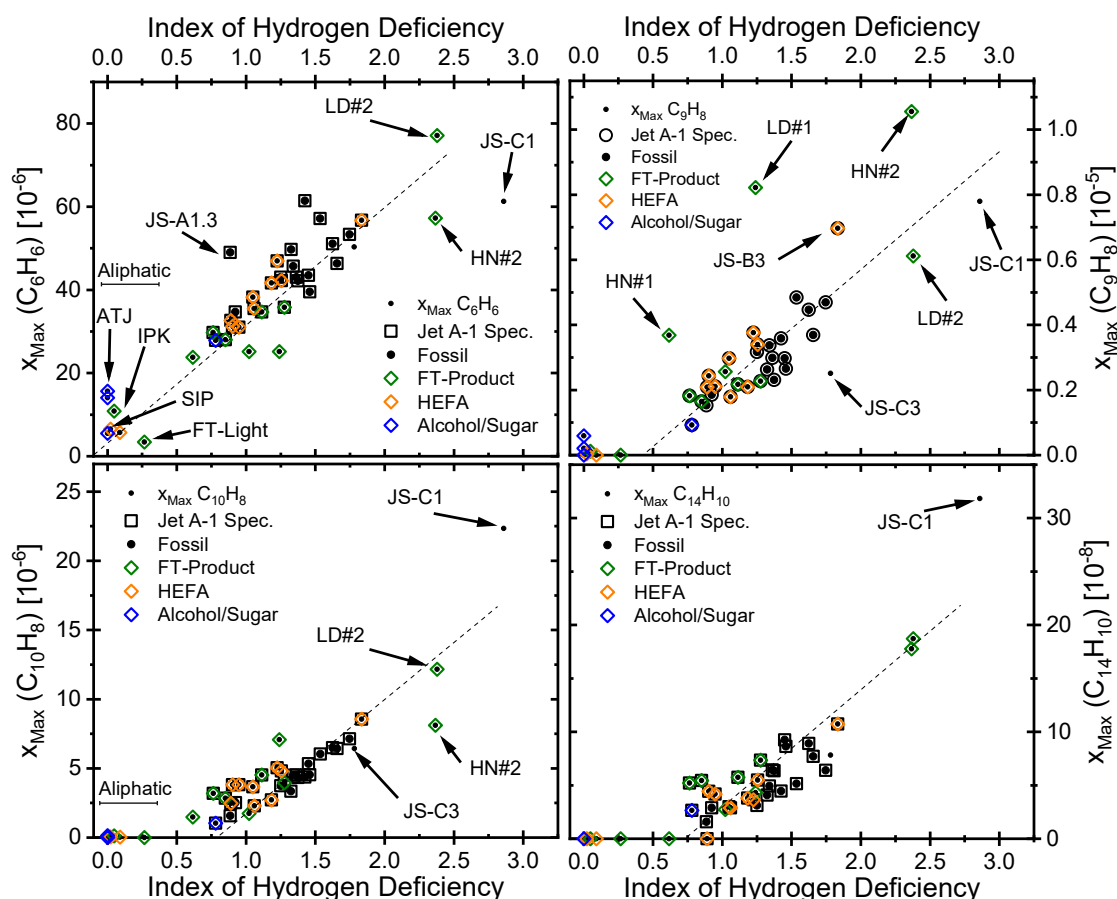
340 Equation 1 shows that the IHD scales linearly with the hydrogen content when the molecule size does  
 341 not change significantly. Technical fuels, in particular those within the jet fuel specification exhibit  
 342 a quite similar molar mass. However, the IHD gives the advantage to enable comparison even with  
 343 fuels of a wider range and will set the pure aliphatic compounds to zero. In Fig. 5 the peak mole  
 344 fractions of important soot precursor intermediates such as benzene ( $\text{C}_6\text{H}_6$ ), indene ( $\text{C}_9\text{H}_8$ ),  
 345 naphthalene ( $\text{C}_{10}\text{H}_8$ ), and phenanthrene/anthracene ( $\text{C}_{14}\text{H}_{10}$ ) are shown. These soot precursors show  
 346 a convincing correlation with the IHD. For benzene the linear regression would give a line through  
 347 origin, while the higher soot precursors show a slight shift to larger IHDs with a similar slope. This  
 348 finding is true for all other detected aromatic soot precursor intermediates here. Since the molecular  
 349 mass of the investigated fuels is in a narrow range, a similar conclusion can also be drawn for the  
 350 hydrogen content (not shown).

351 In general, the fuels containing alternative components exhibit lower soot precursor concentrations  
 352 compared to fossil fuels and support the soot reducing properties reported in many field experiments  
 353 [25, 26]. Following the expectations, aliphatic fuels (IHD~0) exhibit the lowest concentrations in  
 354 soot precursors. For the larger soot precursors (naphthalene and above) they are even close or below  
 355 the detection limit and appear to be negligible compared to other fuels. Only for the aromatic free

356 fuels a dependency of the soot precursors with fuel's iso-alkane content can be drawn [43]. The  
357 heavily branched ATJ exhibits the highest benzene concentration followed by the SASOL-IPK,  
358 HEFA and farnesane (SIP) and the lowest concentration is seen for the n-alkane rich FT-Light. This  
359 FT-crude product also has a noticeable alkene content shifting the IHD above zero. However, the  
360 alkene content seems not to influence the soot precursor chemistry significantly in this case. The  
361 measured peak mole fraction is comparable to neat decane [24].

362 The largest amount of soot precursor species was found for the hydrogen-lean FT-product streams  
363 and the academic surrogates. Namely SASOL-LD#2, SASOL-HN#2 and Jetscreen surrogate JS-C1.  
364 None of these fuels are covered by the ASTM standard, but are of high interest for this systematic  
365 consideration. While SASOL-LD#2 follows the extrapolated trend of certified fuels, SASOL-HN#2  
366 and JS-C1 fall below this trend when mono aromatic soot precursor species are considered (i.e.  
367 benzene). This can be potentially linked to an extraordinary content of multi-ring naphthenic (di- and  
368 tri- cycloalkanes) species in these fuels. The hydrotreated Jetscreen A1.3 also exhibits an increase  
369 benzene concentration. This behavior could be attributed to the hydrogenation of diaromatics towards  
370 bicyclic naphthene's [49].

371 Interestingly the SASOL-HN#2 achieves its IHD by a high amount of mono-aromatic species while  
372 the JS-C1 does by di-aromatics. JS-C1 consequently overshoots the trend or naphthalene while  
373 smaller aromatics are formed in subpar amount. SASOL-LD#2 exhibits a balanced mixture and  
374 consequently follows the trend. The disproportionately high levels of indene ( $C_9H_8$ ) at the fuels  
375 HN#1, HN#2 and JS-B3 (ReadiJet) can be linked to the noticeable amounts of indane ( $C_9H_{10}$ ) content  
376 of the fuels. It is further noticeable that the differences between the highly unsaturated fuels vanish  
377 when higher soot precursor species are considered.

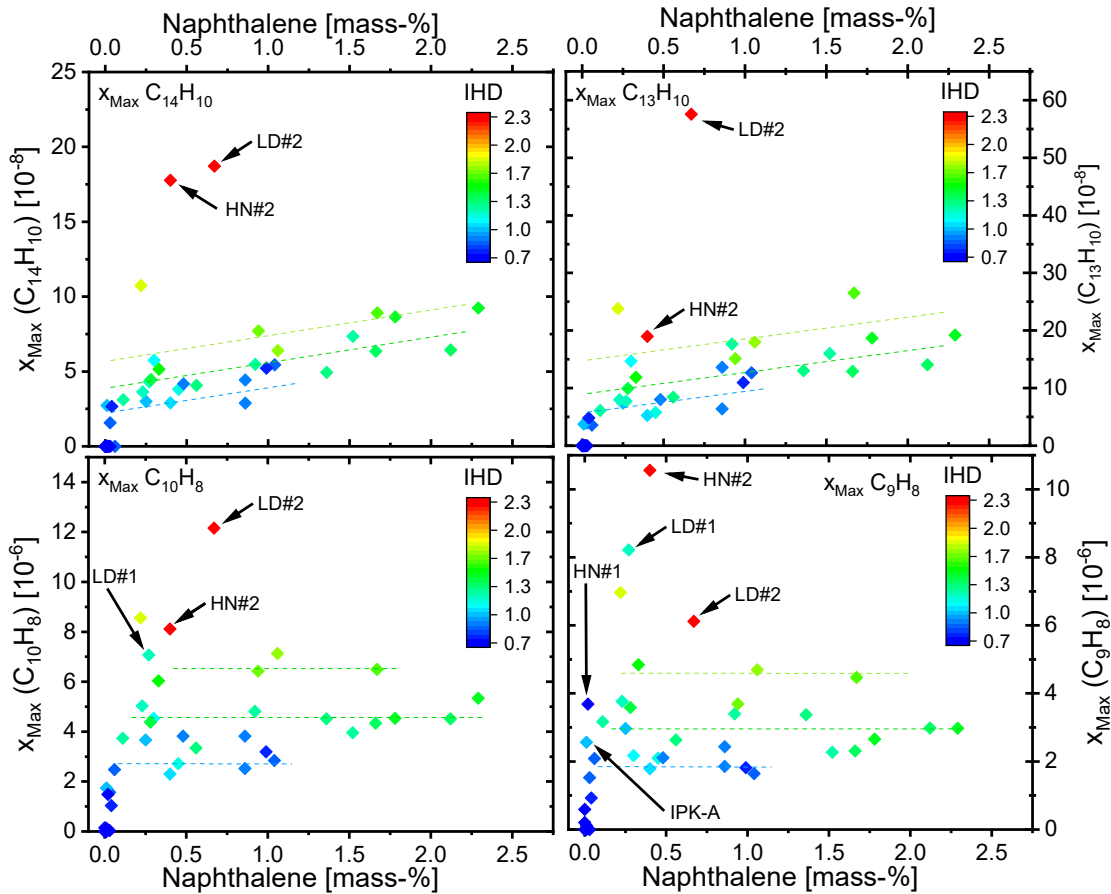


378

379 **Figure 5:** Peak mole fractions ( $\Phi=1.2$ ) of the soot precursor intermediates benzene ( $C_6H_6$ ), indene ( $C_9H_8$ ),  
 380 naphthalene ( $C_{10}H_8$ ), and phenanthrene/anthracene ( $C_{14}H_{10}$ ) as a function of the degree of unsaturation  
 381 expressed in IHD. Fuels fulfilling ASTM requirements are highlighted by black squares, colors indicate the  
 382 respective group according to table 1. Lines are drawn to guide the eye.

383 The amount of di-aromatics (naphthalenes) is often correlated to the sooting tendency of a technical  
 384 fuel. To a certain extent the IHD or hydrogen content also covers the naphthalene content of the fuel,  
 385 since multi-ring aromatics have a higher IHD or lower hydrogen content. Indeed, an influence of the  
 386 naphthalene content beyond the IHD cannot be drawn for small soot precursors. However, when  
 387 multi-ring aromatics are considered, a noticeable correlation can be verified. Figure 6 gives the peak  
 388 mole fractions of phenanthrene/anthracene ( $C_{14}H_{10}$ ), fluorene ( $C_{13}H_{10}$ ), naphthalene ( $C_{10}H_8$ ) and  
 389 indane ( $C_9H_8$ ) as a function of the naphthalene content of the fuel. It should be noted that the applied  
 390 naphthalene test (ASTM-D1840) measures the mass fraction of the sum of all di-aromatic species  
 391 based on an assumed absorption cross section typical for conventional mineral oil products. The peak  
 392 mole fractions of  $C_{14}H_{10}$  clearly rise with increasing naphthalene content within fuels of similar IHD  
 393 (same color). Additionally, the level of this gain increases within increasing IHD as shown in Fig. 6.

394 A similar behavior can be stated for  $C_{13}H_{10}$ . For SASOL-LD#2 a remarkably high  $C_{13}H_{10}$   
 395 concentration was measured while at the same time indene is relatively low. This might be linked to  
 396 the significant amount of tricyclic-paraffins contained in this fuel. For  $C_{10}H_8$  and smaller soot  
 397 precursor intermediates (e.g.  $C_9H_8$ ) no distinct correlation to the naphthalene content can be seen.  
 398 The detected concentration rises only by the increase of IHD as visualized in Fig. 5.



399  
 400 **Figure 6:** Peak mole fractions ( $\Phi=1.2$ ) of poly-aromatic soot precursor species  $C_{14}H_{10}$ ,  $C_{13}H_{10}$ ,  $C_{10}H_8$  and  $C_9H_8$   
 401 as function of the naphthalene content (ASTM-D1840) the IHD (Index of Hydrogen Deficiency) of the  
 402 respective fuel is color-coded. Lines are drawn to guide the eye.

403

## 404      **5. Summary**

405      Part-I of our trilogy on alternative aviation fuels covers the experimental framework for the  
406      subsequent modeling approach. A respective collection on over 40 technical fuel samples is  
407      presented and characterized here providing the basis for experimental and modeling work of this  
408      trilogy.

409      Detailed examination is provided by measurements at the DLR high-temperature flow reactor. Fuels  
410      are selected from numerous national and international large-scale projects, which can be linked to a  
411      large number of complementary experiments like engine or inflight emission measurements.  
412      Quantitative evolution of combustion reaction intermediates is recorded for slightly rich ( $\Phi=1.2$ ) and  
413      lean ( $\Phi=0.8$ ) conditions. This unique dataset provides systematic insights on the influence of the  
414      chemical composition on the combustion kinetics of chemically complex fuels and is available for  
415      further model development from the authors upon request.

416      The general reaction behavior was found to be almost identical when fuels fulfill the current  
417      specification. Also fuel decay was observed to be widely independent from the fuel composition and  
418      the consumption of different chemical classes are similar in most fuels but each class shows an  
419      individual decomposition behavior. The influence of the chemical composition of the fuel on the  
420      intermediate species pool was examined. The structure of alkanes (e.g. branched vs. linear) as major  
421      constituent of most fuels, was seen to dominate the intermediate species pool solely when no other  
422      chemical classes are present.

423      Special attention was given to the soot precursor chemistry of the fuels. A general systematic  
424      dependency of the soot precursor concentration on the degree of unsaturation IHD (Index of  
425      Hydrogen Deficiency) or the hydrogen content respectively, was demonstrated. Beyond this,  
426      additional increases of larger soot precursor species with the fuels' naphthalene (di-aromatic) content  
427      were shown. To the best of our knowledge this is the first time that this relationship was  
428      systematically proven for complex technical fuels on a molecular level. This will be covered in Part-II

429 [42] from a modeling point of view with the presentation of the elaborate surrogate modeling  
430 approach, followed by the application on technical fuels presented here in Part-III [43] of this series.

### 431 **Acknowledgements**

432 Tim Edwards for providing the NJFCP fuels and Marc Mühlberg for his experimental contributions  
433 are gratefully acknowledged. DLR has received funding from the European Union's Horizon 2020  
434 research and innovation program under grant agreement No 723525 (JETSCREEN). Don't Panic!

435

- 437 [1] Wang M, Dewil R, Maniatis K, Wheeldon J, Tan T, Baeyens J, et al. Biomass-derived  
438 aviation fuels: Challenges and perspective. *Prog Energy Combust Sci* 2019;74:31-49.  
439 <https://doi.org/10.1016/j.pecs.2019.04.004>
- 440 [2] Drünert S, Neuling U, Zitscher T, Kaltschmitt M. Power-to-Liquid fuels for aviation –  
441 Processes, resources and supply potential under German conditions. *Applied Energy*  
442 2020;277. <https://doi.org/10.1016/j.apenergy.2020.115578>
- 443 [3] Doliente SS, Narayan A, Tapia JFD, Samsatli NJ, Zhao Y, Samsatli S. Bio-aviation Fuel: A  
444 Comprehensive Review and Analysis of the Supply Chain Components. *Frontiers in Energy*  
445 *Research* 2020;8. <https://doi.org/10.3389/fenrg.2020.00110>
- 446 [4] Lobo P, Hagen DE, Whitefield PD. Comparison of PM emissions from a commercial jet  
447 engine burning conventional, biomass, and Fischer-Tropsch fuels. *Environ Sci Technol*  
448 2011;45(24):10744-9. <https://doi.org/10.1021/es201902e>
- 449 [5] Brem BT, Durdina L, Siegerist F, Beyerle P, Bruderer K, Rindlisbacher T, et al. Effects of  
450 Fuel Aromatic Content on Nonvolatile Particulate Emissions of an In-Production Aircraft  
451 Gas Turbine. *Environ Sci Technol* 2015;49(22):13149-57.  
452 <https://doi.org/10.1021/acs.est.5b04167>
- 453 [6] Moore RH, Thornhill KL, Weinzierl B, Sauer D, D'Ascoli E, Kim J, et al. Biofuel blending  
454 reduces particle emissions from aircraft engines at cruise conditions. *Nature*  
455 2017;543(7645):411-5. <https://doi.org/10.1038/nature21420>
- 456 [7] Kleine J, Voigt C, Sauer D, Schlager H, Scheibe M, Jurkat-Witschas T, et al. In Situ  
457 Observations of Ice Particle Losses in a Young Persistent Contrail. *Geophys Res Lett*  
458 2018;45(24):13,553-13,61. <https://doi.org/10.1029/2018gl079390>
- 459 [8] Moore RH, Shook MA, Ziemba LD, DiGangi JP, Winstead EL, Rauch B, et al. Take-off  
460 engine particle emission indices for in-service aircraft at Los Angeles International Airport.  
461 *Sci Data* 2017;4:170198. <https://doi.org/10.1038/sdata.2017.198>
- 462 [9] Speth RL, Rojo C, Malina R, Barrett SRH. Black carbon emissions reductions from  
463 combustion of alternative jet fuels. *Atmos Environ* 2015;105:37-42.  
464 <https://doi.org/10.1016/j.atmosenv.2015.01.040>
- 465 [10] Schripp T, Anderson B, Crosbie EC, Moore RH, Herrmann F, Osswald P, et al. Impact of  
466 Alternative Jet Fuels on Engine Exhaust Composition During the 2015 ECLIF Ground-  
467 Based Measurements Campaign. *Environ Sci Technol* 2018;52(8):4969-78.  
468 <https://doi.org/10.1021/acs.est.7b06244>
- 469 [11] Christie S, Lobo P, Lee D, Raper D. Gas Turbine Engine Nonvolatile Particulate Matter  
470 Mass Emissions: Correlation with Smoke Number for Conventional and Alternative Fuel  
471 Blends. *Environ Sci Technol* 2017;51(2):988-96. <https://doi.org/10.1021/acs.est.6b03766>
- 472 [12] Curran HJ. Developing detailed chemical kinetic mechanisms for fuel combustion. *Proc*  
473 *Combust Inst* 2018. <https://doi.org/10.1016/j.proci.2018.06.054>
- 474 [13] Wang H, Xu R, Wang K, Bowman CT, Hanson RK, Davidson DF, et al. A physics-based  
475 approach to modeling real-fuel combustion chemistry - I. Evidence from experiments, and  
476 thermodynamic, chemical kinetic and statistical considerations. *Combust Flame*  
477 2018;193:502-19. <https://doi.org/10.1016/j.combustflame.2018.03.019>
- 478 [14] Xu R, Wang K, Banerjee S, Shao J, Parise T, Zhu Y, et al. A physics-based approach to  
479 modeling real-fuel combustion chemistry – II. Reaction kinetic models of jet and rocket  
480 fuels. *Combust Flame* 2018;193:520-37.  
481 <https://doi.org/10.1016/j.combustflame.2018.03.021>
- 482 [15] Won SH, Haas FM, Dooley S, Edwards T, Dryer FL. Reconstruction of chemical structure  
483 of real fuel by surrogate formulation based upon combustion property targets. *Combust*  
484 *Flame* 2017;183:39-49. <https://doi.org/10.1016/j.combustflame.2017.04.032>
- 485 [16] Abdul Jameel AG, Naser N, Issayev G, Touitou J, Ghosh MK, Emwas A-H, et al. A  
486 minimalist functional group (MFG) approach for surrogate fuel formulation. *Combust Flame*  
487 2018;192:250-71. <https://doi.org/10.1016/j.combustflame.2018.01.036>

- 488 [17] Haylett DR, Davidson DF, Hanson RK. Ignition delay times of low-vapor-pressure fuels  
489 measured using an aerosol shock tube. *Combust Flame* 2012;159(2):552-61.  
490 <https://doi.org/10.1016/j.combustflame.2011.08.021>
- 491 [18] Ji C, Wang YL, Egolfopoulos FN. Flame Studies of Conventional and Alternative Jet Fuels.  
492 *J Propul Power* 2011;27(4):856-63. <https://doi.org/10.2514/1.B34105>
- 493 [19] Richter S, Braun-Unkloff M, Naumann C, Riedel U. Paths to alternative fuels for aviation.  
494 *CEAS Aeronaut J* 2018;9(3):389-403. <https://doi.org/10.1007/s13272-018-0296-1>
- 495 [20] Dagaut P, Cathonnet M. The ignition, oxidation, and combustion of kerosene: A review of  
496 experimental and kinetic modeling. *Prog Energy Combust Sci* 2006;32(1):48-92.  
497 <https://doi.org/10.1016/j.pecs.2005.10.003>
- 498 [21] Dagaut P, Diévar P. Combustion of synthetic jet fuels: Naphthenic cut and blend with a gas-  
499 to-liquid (GtL) jet fuel. *Proceedings of the Combustion Institute* 2017;36(1):433-40.  
500 <https://doi.org/10.1016/j.proci.2016.05.045>
- 501 [22] Dooley S, Won SH, Chaos M, Heyne J, Ju Y, Dryer FL, et al. A jet fuel surrogate formulated  
502 by real fuel properties. *Combust Flame* 2010;157(12):2333–9.  
503 <https://doi.org/10.1016/j.combustflame.2010.07.001>
- 504 [23] Oßwald P, Köhler M. An atmospheric pressure high-temperature laminar flow reactor for  
505 investigation of combustion and related gas phase reaction systems. *Rev Sci Instrum*  
506 2015;86(10):105109. <https://doi.org/10.1063/1.4932608>
- 507 [24] Jürgens S, Oßwald P, Selinsek M, Piermartini P, Schwab J, Pfeifer P, et al. Assessment of  
508 combustion properties of non-hydroprocessed Fischer-Tropsch fuels for aviation. *Fuel*  
509 *Process Technol* 2019;193:232-43. <https://doi.org/10.1016/j.fuproc.2019.05.015>
- 510 [25] Moore RH, Shook M, Beyersdorf A, Corr C, Herndon S, Knighton WB, et al. Influence of  
511 Jet Fuel Composition on Aircraft Engine Emissions: A Synthesis of Aerosol Emissions Data  
512 from the NASA APEX, AAFEX, and ACCESS Missions. *Energy Fuels* 2015;29(4):2591-  
513 600. <https://doi.org/10.1021/ef502618w>
- 514 [26] Schripp T, Herrmann F, Oßwald P, Köhler M, Zschocke A, Weigelt D, et al. Particle  
515 emissions of two unblended alternative jet fuels in a full scale jet engine. *Fuel*  
516 2019;256:115903. <https://doi.org/10.1016/j.fuel.2019.115903>
- 517 [27] Won SH, Dooley S, Veloo PS, Wang H, Oehlschlaeger MA, Dryer FL, et al. The combustion  
518 properties of 2,6,10-trimethyl dodecane and a chemical functional group analysis. *Combust*  
519 *Flame* 2014;161(3):826-34. <https://doi.org/10.1016/j.combustflame.2013.08.010>
- 520 [28] Richter S, Kathrotia T, Naumann C, Kick T, Slavinskaya N, Braun-Unkloff M, et al.  
521 Experimental and modeling study of farnesane. *Fuel* 2018;215:22-9.  
522 <https://doi.org/10.1016/j.fuel.2017.10.117>
- 523 [29] Zschocke A, Scheuermann S, Ortner J. High biofuel blends in aviation (HBBA). 2012.  
524 [https://doi.org/S0016-2361\(19\)31255-4/h0080](https://doi.org/S0016-2361(19)31255-4/h0080)
- 525 [30] Schripp T, Grein T, Zinsmeister J, Oßwald P, Köhler M, Müller-Langer F, et al. Technical  
526 application of a ternary alternative jet fuel blend – Chemical characterization and impact on  
527 jet engine particle emission. *Fuel* 2020;in Press. <https://doi.org/10.1016/j.fuel.2020.119606>
- 528 [31] Edwards JT. Reference Jet Fuels for Combustion Testing. 55th AIAA Aerospace Sciences  
529 Meeting. 2017.
- 530 [32] Bullerdiek N, Buse J, Dögnitz N, Feige A, Halling A-M, Hauschild S, et al. Einsatz von  
531 Multiblend-JET-A-1 in der Praxis, DEMO-SPK final report (in German). BMVI; 2019.
- 532 [33] Rauch B, al. e. JET Fuel SCREENing and Optimization  
533 <https://cordis.europa.eu/project/id/723525>. 2020.
- 534 [34] Riazi MR. Lee-Kesler Method from Characterization and Properties of Petroleum Fractions.  
535 ASTM International; 2005.
- 536 [35] Herrmann F, Jochim B, Oßwald P, Cai L, Pitsch H, Kohse-Höinghaus K. Experimental and  
537 numerical low-temperature oxidation study of ethanol and dimethyl ether. *Combust Flame*  
538 2014;161(2):384-97. <https://doi.org/10.1016/j.combustflame.2013.09.014>
- 539 [36] Köhler M, Oßwald P, Xu H-B, Kathrotia T, Hasse C, Riedel U. Speciation data for fuel-rich  
540 methane oxy-combustion and reforming under prototypical partial oxidation conditions.  
541 *Chem Eng Sci* 2016;139:249-60. <https://doi.org/10.1016/j.ces.2015.09.033>

- 542 [37] Oßwald P, Whitside R, Schäffer J, Köhler M. An experimental flow reactor study of the  
543 combustion kinetics of terpenoid jet fuel compounds: Farnesane, p-menthane and p-cymene.  
544 Fuel 2017;187:43-50. <https://doi.org/10.1016/j.fuel.2016.09.035>
- 545 [38] Chu TC, Buras ZJ, Oßwald P, Liu M, Goldman MJ, Green WH. Modeling of aromatics  
546 formation in fuel-rich methane oxy-combustion with an automatically generated pressure-  
547 dependent mechanism. Phys Chem Chem Phys 2019;21(2):813-32.  
548 <https://doi.org/10.1039/c8cp06097e>
- 549 [39] Biordi JC. Molecular beam mass spectrometry for studying the fundamental chemistry of  
550 flames. Prog Energy Combust Sci 1977;3(3):151-73. [https://doi.org/10.1016/0360-1285\(77\)90002-8](https://doi.org/10.1016/0360-1285(77)90002-8)
- 551 [40] Oßwald P, Hemberger P, Bierkandt T, Akyildiz E, Köhler M, Bodi A, et al. In situ flame  
552 chemistry tracing by imaging photoelectron photoion coincidence spectroscopy. Rev Sci  
553 Instrum 2014;85(2 ):025101. <https://doi.org/10.1063/1.4861175>
- 554 [41] Krüger D, Oßwald P, Köhler M, Hemberger P, Bierkandt T, Karakaya Y, et al. Hydrogen  
555 abstraction ratios: A systematic iPEPICO spectroscopic investigation in laminar flames.  
556 Combust Flame 2018;191:343-52. <https://doi.org/10.1016/j.combustflame.2017.12.025>
- 557 [42] Kathrotia T, Oßwald P, Naumann C, Richter S, Köhler M. Combustion Kinetics of  
558 Alternative Jet Fuels, Part-II: Reaction Model for Fuel Surrogate. Manuscript submitted to  
559 Fuel 2020.
- 560 [43] Kathrotia T, Oßwald P, Zinsmeister J, Methling T, Köhler M. Combustion Kinetics of  
561 Alternative Jet Fuels, Part-III: Fuel Modeling and Surrogate Strategy. Manuscript submitted  
562 to Fuel 2020.
- 563 [44] Kathrotia T, Oßwald P, Köhler M, Slavinskaya N, Riedel U. Experimental and mechanistic  
564 investigation of benzene formation during atmospheric pressure flow reactor oxidation of n-  
565 hexane, n-nonane, and n-dodecane below 1200 K. Combust Flame 2018;194:426-38.  
566 <https://doi.org/10.1016/j.combustflame.2018.05.027>
- 567 [45] Kathrotia T, Naumann C, Oßwald P, Köhler M, Riedel U. Kinetics of Ethylene Glycol: The  
568 first validated reaction scheme and first measurements of ignition delay times and speciation  
569 data. Combust Flame 2017;179:172-84.  
570 <https://doi.org/10.1016/j.combustflame.2017.01.018>
- 571 [46] Hadaller OJ, Johnson JM. CRC Report No. 647: World Fuel Sampling Program. CRC  
572 Aviation Fuel, Lubricant & Equipment Research Committee of the Coordinating Research  
573 Council, Inc; 2006.
- 574 [47] Minchin ST. Luminous Stationary Flames: the Quantitative Relationship between Flame  
575 Dimensions at the Sooting Point and Chemical Composition, with Special Reference to  
576 Petroleum Hydrocarbons. J Inst Petr Techn 1931;17:S. 102-20.
- 577 [48] Kathrotia T, Riedel U. Predicting the soot emission tendency of real fuels – A relative  
578 assessment based on an empirical formula. Fuel 2020;261:116482.  
579 <https://doi.org/10.1016/j.fuel.2019.116482>
- 580 [49] Pelucchi M, Oßwald P, Pejpichestakul W, Frassoldati A, Mehl M. On the combustion and  
581 sooting behavior of standard and hydro-treated jet fuels: An experimental and modeling  
582 study on the compositional effects. Proc Combust Inst 2020.  
583 <https://doi.org/10.1016/j.proci.2020.06.353>
- 584

585